

Optical Properties of Gold Nanorods: DDA Simulations Supported by Experiments

A. Brioude, X. C. Jiang, and M. P. Pileni*

Laboratoire LM2N, Université P. et M. Curie (Paris VI), BP 52, 4 Place Jussieu,
F - 75231 Paris Cedex 05, France

Received: February 10, 2005; In Final Form: March 21, 2005

Simulations of the absorption efficiency using the discrete dipole approximation (DDA) method and taking into account the real shape of gold nanorods are reported. A dominant surface plasma band corresponding to the longitudinal resonance is observed. Its maximum position λ_{\max} shifts to the red as the aspect ratio increases. The transversal dipolar and multipolar mode wavelength positions are also discussed. These data are in good agreement with previous theoretical work based on classical electrostatic predictions and assuming that gold nanorods behave as ellipsoidal particles. From the experimental point of view, good agreement with the published data for gold nanorods is obtained.

I. Introduction

There is currently a great deal of interest in metallic nanorods due to their shape-dependent optoelectronic properties,¹ such as strong surface-enhanced Raman scattering (SERS),² fluorescence,³ and anisotropic chemical reactivity,⁴ all of which can be used in various applications. Gold nanorods, as a typical example, have been given much more attention due to their stability and sensibility in biochemistry and have become promising candidates for sensing or imaging applications.⁵ To date, a number of investigations for synthesizing gold nanorods have been reported including a porous aluminum oxide membrane,⁶ an electrochemical method with surfactant molecules as directing agents,⁷ a seed-mediated growth method with the aid of cetyltrimethylammonium bromide (CTAB),⁸ and a photochemical method.⁹ Among these methods, the seed-mediated route has been widely investigated by several groups.^{8a,b,10} However, the rod formation mechanism is still not very clearly understood because the reaction system for particle elongation seems to be very complicated. A slight change in the content of any single component such as HAuCl_4 , AgNO_3 , reducing agents (L-ascorbic acid, NaBH_4), surfactant (CTAB), or seed would lead to a large change in the morphology and the size of the nanorods.

The discrete dipole approximation (DDA) method¹¹ has been extensively developed in the past few years for the specific study of nonspherical nanoparticles. Recently, a number of groups have compared the optical properties obtained from experiments and DDA simulations for silver nanoprisms,¹² silver nanodisks,¹³ and copper nanocrystals with arbitrary shapes.¹⁴

Here, simulations using the DDA for Au nanorods are reported. They are compared to previous theoretical work based on the classical electrostatic approach.^{15,16} Very recent experimental data obtained by other groups are also explained with the DDA method.^{12–14} The main idea underlying our approach is that the well-matched simulation with respect to the experimental observations could clearly explain each resonance plasmon band appearing in the absorption spectrum.

II. DDA Simulations

The DDA method is a numerical method first introduced by Purcell and Pennypacker¹⁷ in which the object studied is represented as a cubic lattice of N polarizable point dipoles localized at r_i , $i = 1, 2, \dots, N$, each one characterized by a polarizability α_i . There is no restriction on the localization of cubic lattice sites so that the DDA represents a particle of arbitrary shape and composition. The object is excited by a monochromatic incident plane wave $\mathbf{E}_{\text{inc}}(r, t) = \mathbf{E}_0 e^{i\mathbf{k}\cdot\mathbf{r} - i\omega t}$, where r , t , w , $k = w/c = 2\pi/\lambda$, c , and λ are the position vector, the time, the angular frequency, the wave vector, the speed of light, and the wavelength of the incident light, respectively. Each dipole of the system is subjected to an electric field consisting of two main contributions: the incident radiation field $\mathbf{E}_{\text{inc},i}$ and the field radiated by all other induced dipoles $\mathbf{E}_{\text{dip},i}$. The local field at each dipole is then given by eq 1.

$$\mathbf{E}_{i,\text{loc}} = \mathbf{E}_{\text{inc},i} + \mathbf{E}_{\text{dip},i} = \mathbf{E}_0 e^{i\mathbf{k}\cdot\mathbf{r}_i} - \sum_{i \neq j} \mathbf{A}_{ij} \cdot \mathbf{P}_j \quad (1)$$

\mathbf{P}_i is the dipole moment of the i th element, and \mathbf{A}_{ij} with $i \neq j$ is an interaction matrix with $3N \times 3N$ matrices as elements described by eq 2.

$$\mathbf{A}_{ij} \cdot \mathbf{P}_j = \frac{e^{ikr_{ij}}}{r_{ij}^3} \left\{ k^2 \mathbf{r}_{ij} \times (\mathbf{r}_{ij} \times \mathbf{P}_j) + \frac{(1 - ikr_{ij})}{r_{ij}^2} [r_{ij}^2 \mathbf{P}_j - 3\mathbf{r}_{ij}(\mathbf{r}_{ij} \cdot \mathbf{P}_j)] \right\} \quad (2)$$

The $3N$ -coupled complex linear equations given by eq 3 are solved, and each dipole moment \mathbf{P}_i is determined.

$$\mathbf{P}_i = \alpha_i \cdot \mathbf{E}_{i,\text{loc}} \quad (3)$$

The absorption cross sections for a defined target in terms of dipole moments can be derived:

$$C_{\text{abs}} = \frac{4\pi k}{|\mathbf{E}_0|^2} \sum_{i=1}^N \left\{ \text{Im}[\mathbf{P}_i \cdot (\alpha_i^{-1})^* \mathbf{P}_i^*] - \frac{2}{3} k^3 |\mathbf{P}_i|^2 \right\} \quad (4)$$

* To whom correspondence should be addressed. E-mail: pileni@sri.jussieu.fr.

where * means the complex conjugate. We defined the absorption efficiencies as $Q_{\text{abs}} = C_{\text{abs}}/A$, where $A = \pi a_{\text{eff}}^2$, and a_{eff} is defined through the concept of an effective volume equal to $4\pi a_{\text{eff}}^3/3$.

In all the calculations presented here, we consider gold nanoparticles described by the dielectric function ϵ_i measured by Palik.¹⁸

The surrounding media dielectric constant enters into the calculation through a factor ϵ_0 which is contained in the polarizability α_i . The explicit formula for α_i was developed by Draine and Goodman.¹⁹ To match the experimental conditions of gold nanorod synthesis, the dielectric constant ϵ_0 used in the calculations is 1.77, which corresponds to the value for water where the nanorods are dissolved. Compared to simulations obtained in a vacuum, and reported, in general, in other papers,^{2,11} a significant nonlinear red shift of plasmon resonances is observed.

To solve the complex linear equations in the DDA, the code adapted by Draine and Flatau²⁰ is used. In actual practice, there are significant advantages associated with summing over the dipole fields in eq 1 using the fast Fourier transform method,¹⁹ and in substituting eqs 1 and 2 into eq 3, we obtain a relation of the form $A' \cdot P = E$ that we can solve with the complex conjugate gradient techniques. A' is a $3N \times 3N$ matrix built from A , and for a system with a total of N elements, E and P are $3N$ -dimensional vectors. One of the advantages of this technique is that it allows a certain arbitrariness in the construction of the array of dipole points that represent the studied target of a given geometry. For example, the geometry of the grid where dipoles have to be located is usually chosen to be cubic but it is not uniquely determined. Obviously, the gridding associated with the DDA calculation created distortion of the rod surfaces, but except for the layer closest to the surface, fields are smooth and well converged. In a recent publication,^{11b} the question of the number of dipoles needed to mimic the continuum macroscopic particle (to approach a homogeneous particle) with an array of discrete dipoles is treated. The answer is not straightforward, because the convergence of physical quantities is related to this number. Typically, cross sections calculated with the DDA are accurate to a few percent if $N \geq 10^4$ dipoles are used. To avoid problems with the accuracy of the simulations, a very large number of dipoles (40 000) have been used for calculations. As presented previously, we have a matrix of $(3N)^2$ complex elements that would require a large amount of computational effort.

III. Results and Discussion

In the following, theoretical calculations of the absorption efficiencies using the DDA method are compared to experiments either published (see refs 8d, 21, and 22) or presented below.

The major change in the absorption spectrum of gold nanorods is the position of the well-known longitudinal mode LM. To find the influence on the resonance maximum λ_{max} of the geometrical parameters of nanorods such as width W , length L , and aspect ratio AR, defined by the length divided by the width, a batch of simulations, considering each parameter, is performed.

Let us first consider gold nanorods having a fixed width ($W = 7.5$ nm) and various lengths—25, 40, and 50 nm. The λ_{max} values of the LM mode appear at 773, 984, and 1159 nm, respectively (Figure 1A). Upon increasing the width to $W = 15$ nm, the λ_{max} values of the LM mode are centered at 661, 722, and 780 nm, respectively (Figure 1B). The simulated

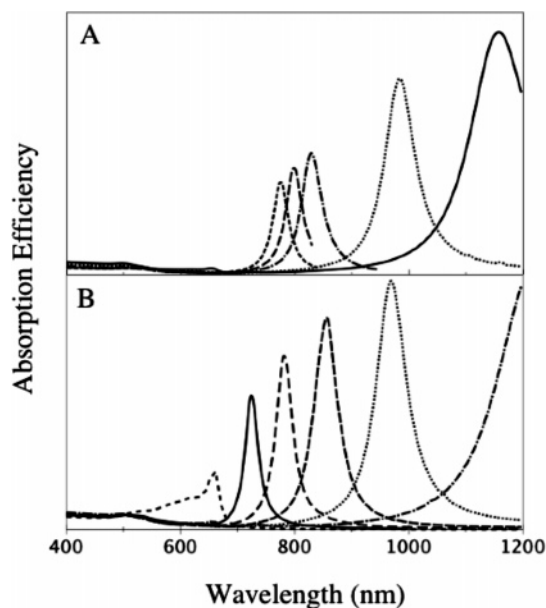


Figure 1. (A) Simulated absorption spectra of nanorods with a width of 7.5 nm and the following different lengths: 25 nm (---), 27 nm (- · - ·), 29 nm (· · ·), 40 nm (···), and 50 nm (—). (B) Simulated absorption spectra of nanorods with a width of 15 nm and the following different lengths: 25 nm (---), 40 nm (—), 50 nm (— · —), 60 nm (— · —), 75 nm (···), and 100 nm (— · —).

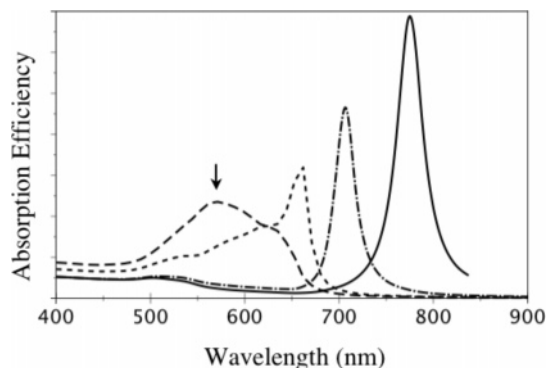


Figure 2. Simulated absorption spectra of nanorods with a length of 25 nm and the following different widths: 20 nm (---), 15 nm (- · - ·), 10 nm (· · ·), and 7.5 nm (—).

absorption spectra obtained at various widths and a fixed length ($L = 25$ nm) show a blue shift of the λ_{max} position (Figure 2). It can thus be concluded that, at a fixed width, the increase in the length induces a red shift of the LM mode maximum. Furthermore, at fixed lengths, the LM mode maximum is blue-shifted upon increasing the width. Hence, the AR is the key parameter in the optical properties of gold nanorods.

The λ_{max} position increases linearly with the nanorod length L . However, the value of the linear increase depends on the width of nanorods. Figure 3A shows a sharper slope for $W = 7.5$ nm (see squares) compared to that obtained for $W = 15$ nm (see triangles). This is confirmed by published experimental data.^{8d,21} Figure 3A reports the slope deduced from the work of Al-Sayed et al.²¹ on gold nanorods with $W = 10$ nm (circles) and that of Pérez Juste et al.^{8d} with $W = 26$ nm (diamonds). In both cases, the experimental conditions are the same as those considered in the calculation (mainly the refractive index of the surrounding media $n = 1.33$). To explain the differences in the slope of λ_{max} versus L , simulations are performed for various widths. Figure 3B shows the slope markedly decreases with W . To a first approximation, we describe the behavior of this slope

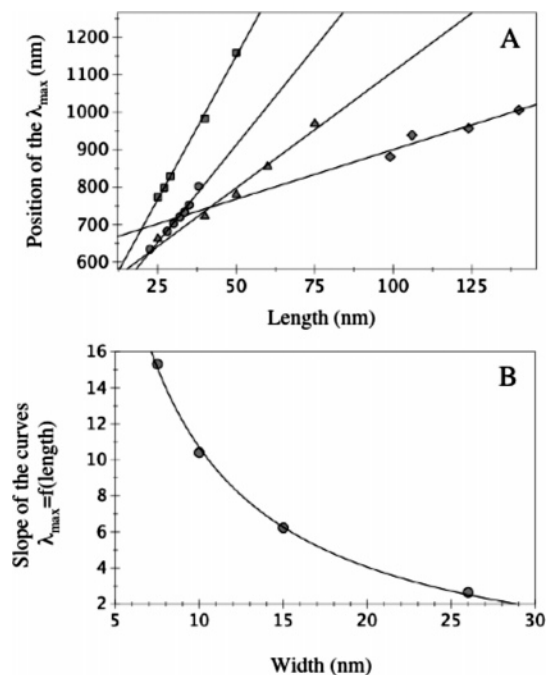


Figure 3. (A) Position of λ_{\max} (nm) versus the nanorod length. Simulation results using the DDA for a width of 7.5 nm (squares), a width of 15 nm (triangles), a width of 10 nm from Al-Sayed et al.²¹ (circles), and a width of 26 nm from Pérez-Juste et al.^{8d} (diamonds). (B) Calculated slope of the related line plotted in part A versus the width W of the nanorods. From left to right, the corresponding circles are for $W = 7.5$ nm, $W = 10$ nm, $W = 15$ nm, and $W = 26$ nm.

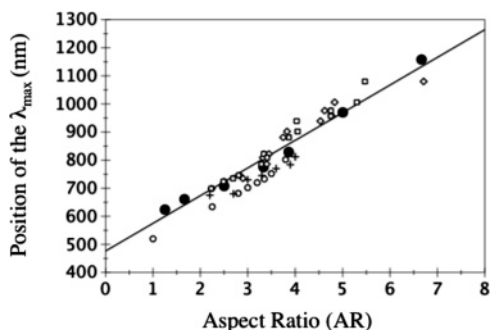


Figure 4. Position of λ_{\max} (nm) versus the aspect ratio of nanorods. Simulation results using the DDA method (black circles) and the corresponding fit (straight line). Experimental data from the work of Al-Sayed et al.²¹ (open circles) and Pérez-Juste et al.^{8d} (diamonds and squares). Experimental data from our study (crosses) extracted from Figure 6.

S versus the nanorod width W by the function

$$S = a/W + b$$

with $a = 133$ and $b = -2.6$. Considering the fact that $W = L/AR$, this equation becomes

$$S = (aAR/L) + b$$

This shows that S linearly increases with AR and is inversely proportional to L .

Figure 4 shows the linear variation of λ_{\max} with AR . The best fit of the simulated data is obtained for the following equation:

$$\lambda_{\max} = 96AR + 418 \quad (5)$$

The above theoretical results are compared with recent experi-

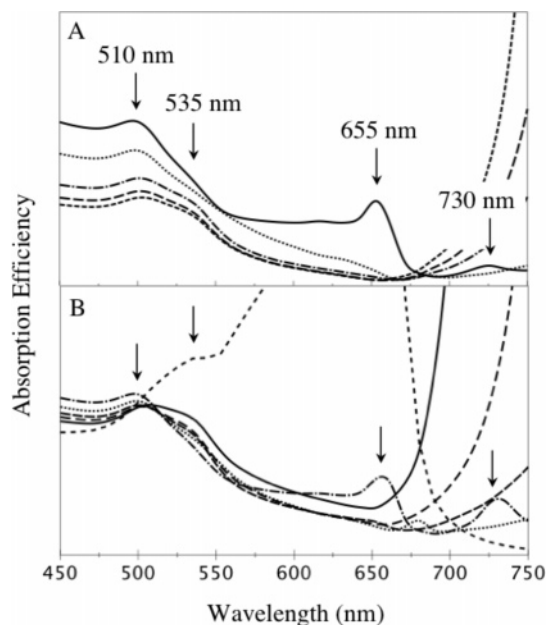


Figure 5. (A) Enlargement of Figure 1A in the range 450–750 nm. (B) Enlargement of Figure 1B in the range 450–750 nm.

mental data from other papers^{8d,21} (diamonds, circles). To confirm this claim, gold nanorods with different aspect ratios are synthesized in our laboratory (see the Appendix). Rather good agreement (see crosses) with the other experiments and simulations presented above is obtained (Figure 4). The slight discrepancy between the wavelength position of the experimental data and the theoretical line can be explained by the fact that the refractive index taken in the simulation ($n = 1.33$) is probably different in the experiments. Al-Sayed et al.²¹ have shown, with a micellar solution of a water/glycerol mixture, that increasing the amount of glycerol in the micellar solution implies a slight red shift of λ_{\max} . In the comments on their paper, Yan et al.²³ derived a simple relationship between the absorption maximum of LM, the aspect ratio AR , and the medium dielectric constant ϵ_0 :

$$\lambda_{\max} = (52.95AR - 41.68)\epsilon_0 + 466.38 \quad (6)$$

Taking into account the refractive index $\epsilon_0 = 1.77$ of the surrounding medium, the previous eq 6 gives $\lambda_{\max} = 93.72AR + 392.6$, which is very close to eq 5 obtained by the DDA method.

We compare the present simulations obtained with the DDA method with simulation results of a model using the Gans theory, that is an extension of the Mie theory with a geometrical factor.^{7b} This theory was first used for elongated particles by Lebedeva et al.,²⁴ and the first experimental evidence supporting the Gans theory was obtained by Skillman et al.²⁵ for silver ellipsoids embedded in gelatin. van der Zande et al.^{7b} using Lebedeva calculations found linear behavior similar to that described before with the same slope. Moreover, the extreme shift of the longitudinal resonances to the longer wavelengths with increasing aspect ratio is clearly observed by Yu et al.^{7a} and is exactly what the electrostatic theory approach^{15,16} predicts for a similar case of gold prolate nanospheroids. In this case, the trend predicted by the classical electrostatic theory is very close to our simulation results.

Up to now, we have not taken the transversal dipolar mode TM or the multipolar resonance mode into account. The well-known position of the TM is determined at 535 nm in Figure 5, which is the corresponding enlargement of Figure 1 in the

TABLE 1: Experimental Conditions and Size of Au Nanorods

Figure 6	aspect ratio	length (nm)	width (nm)	λ_{\max} (nm)	CTAB (M)	H AuCl ₄ (10 ⁻⁴ M)	AgNO ₃ (10 ⁻⁵ M)	[L-aa]/[H AuCl ₄]	[Au] _{seed} /[H AuCl ₄]
A	4.0	28.6	7.1	784	0.095	4.0	6.0	1.6:1	1:320
B	3.7	33.3	9.0	770	0.095	4.0	6.0	1.6:1	1:320
C	3.3	29.8	9.1	736	0.14	2.5	5.0	2:1	1:200
D	3.0	26.5	8.7	720	0.048	2.5	5.0	2:1	1:200
E	2.7	22.9	8.5	688	0.024	2.5	5.0	2:1	1:200
F	2.2	10.7	4.9	668	0.0024	2.5	5.0	2:1	1:200

range 450–750. The assignment of this transversal dipolar mode has been already done by both experimental^{7b} and theoretical work using the Lebedeva calculation.²⁴ In our experimental size range where the nanorod width is inferior to 10 nm, the position of this resonance is unchanged whatever the nanorod length is (Figure 5). Nevertheless, Figure 2 shows that, by increasing this width to 20 nm, this resonance red-shifts and becomes predominant (marked by an arrow). Moreover, Figure 5B shows clearly that, by reducing the aspect ratio of the particles, the intensity of this resonance increases. This is not surprising, since, for an aspect ratio of 1, the two resonance modes TM and LM should be of the same order with only a slight difference in their positions.

Even though these Au nanorods are rather small (in size), multipolar resonance (at least quadrupolar mode) of the LM cannot be excluded in this range. As the near field around the particle is not well described in this approximation, the DDA cannot assign a specific multipolar order to a given geometry.²⁶ Nevertheless, as shown in Figure 5, one can assert that high multipolar excitation intensities marked by arrows are due to size effects because they are more pronounced for large sizes ($L = 50, 100$ nm). Those assumptions are in agreement with previous works on silver cylinders.^{11b} The fact that those multipolar resonance positions are the same for ($W = 7.5$ nm, $L = 50$ nm) and ($W = 15$ nm, $L = 100$ nm) in parts A and B of Figure 5, respectively, can be explained by the similar aspect ratio in the two structures considered.

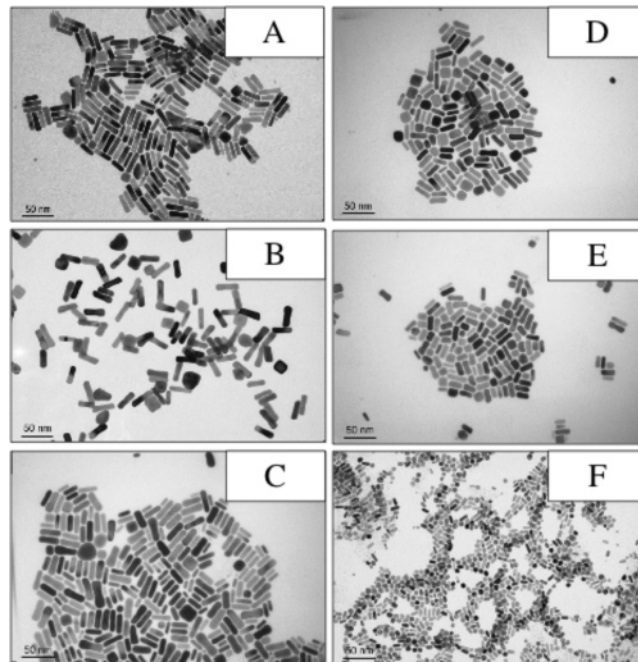
IV. Conclusions

In this paper, we demonstrate that the optical properties of Au nanorods are mainly governed by the longitudinal dipolar mode, that is, by the aspect ratio of the nanocrystals. The simulations presented in this paper are in good agreement with our studies and very recent experimental data and with previous theoretical work based on classical electrostatic prediction and the Gans theory. The DDA approach appears to be a very useful tool for the study of the precise optical properties of nanorods, and for clearly explaining each resonance plasmon band arising in an absorption spectrum.

Acknowledgment. The authors thank Pr. M. El-Sayed who convinced us that we should make further simulations using the DDA method in this study. This work has been supported by a P.I.C.S (Programmes Internationaux de coopérations scientifiques) from CNRS.

Appendix

The gold nanorods are synthesized using the procedure described previously.⁸ Briefly, Au seeds are produced by mixing 1.25 mL of 0.002 M aqueous H AuCl₄ solution and 2.74 mL of 18 MΩ water in a test tube and then adding 3.76 mL of 0.20 M aqueous CTAB solution with further mixing; the color of the mixed solution quickly changes from light yellow to orange. Finally, 0.9 mL of an aqueous 0.01 M NaBH₄ solution at 0 °C

**Figure 6.** TEM images of gold nanorods with different aspect ratios.

is added, followed by shaking the solution vigorously. The growth solution (total volume of 8 mL) contains H AuCl₄·3H₂O (4.0×10^{-4} M), CTAB (0.095 M), and Ag⁺ (6.0×10^{-5} M), and the molar ratio of reducing agent (6.4×10^{-4} M) to [AuCl₄⁻] is kept at 1.6:1, and they are added in a test tube one by one in that order. In the final step, the 2 h aged seed solution is added into the growth solution, and the final seed concentration [Au]_{seed} is 5.0×10^{-7} M. The mixed solution is stirred vigorously for 20 s and then left undisturbed overnight.

Figure 6 shows TEM images²⁷ of gold nanorods with different aspect ratios. The details of each synthesis are given in Table 1. The differences in shape and size of Au nanorods show the limitation in reproducibility under the same conditions (Figure 6A,B). Figure 6C–F shows that the concentration of CTAB plays a crucial role in controlling the shape and size of Au nanoparticles.

References and Notes

- (1) El-Sayed, M. A. *Acc. Chem. Res.* **2001**, *34*, 257.
- (2) Nikoobakht, B.; Wang, Z.; El-Sayed, M. A. *Chem. Phys. Lett.* **2002**, *366*, 17.
- (3) Mohamed, M. B.; Volkov, V.; Link, S.; El-Sayed, M. A. *Chem. Phys. Lett.* **2000**, *317*, 517.
- (4) Jana, N. R.; Gearheart, L.; Obare, S. O.; Murphy, C. J. *Langmuir* **2002**, *18*, 922.
- (5) (a) Haynes, C. L.; Van Duyne, R. P. *J. Phys. Chem. B* **2001**, *105*, 5599. (b) Sönnichsen, C.; Franzl, T.; Wilk, T.; von Plessen, G.; Feldmann, J.; Wilson, O.; Mulvaney, P. *Phys. Rev. Lett.* **2002**, *88*, 077402. (c) Thomas, K. G.; Barazzouk, S.; Ipe, B. I.; Joseph, S. T. S.; Kamat, P. V. *J. Phys. Chem. B* **2004**, *108*, 13066. (d) Gole, A.; Orendorff, C. J.; Murphy, C. J. *Langmuir* **2004**, *20*, 7117. (e) Caswell, K. K.; Wilson, J. N.; Bunz, U. H. F.; Murphy, C. J. *J. Am. Chem. Soc.* **2003**, *125*, 13914. (f) Dujardin, E.; Hsin, L.-B.; Wang, C. R. C.; Mann, S. *Chem. Commun.* **2001**, 1264. (g)

- Wei, Q. H.; Su, K. H.; Durant, S.; Zhang, X. *Nano Lett.* **2004**, *4*, 1067. (h) Nikoobakht, B.; Wang, Z.; El-Sayed, M. A. *J. Phys. Chem. B* **2000**, *104*, 8635.
- (6) Martin, C. R. *Chem. Mater.* **1996**, *8*, 1739.
- (7) (a) Yu, Y.-Y.; Chang, S.-S.; Lee, C.-L.; Wang, C. R. *J. Phys. Chem. B* **1997**, *101*, 6661. (b) van der Zande, B. M. I.; Böhmer, M. R.; Fokkink, L. G. J.; Schönenberger, C. *J. Phys. Chem. B* **1997**, *101*, 852.
- (8) (a) Murphy, C. J.; Jana, N. R. *Adv. Mater.* **2002**, *14*, 80. (b) Nikoobakht, B.; El-Sayed, M. A. *Chem. Mater.* **2003**, *15*, 1957. (c) Jana, N. R.; Gearheart, L.; Murphy, C. J. *J. Phys. Chem. B* **2001**, *105*, 4065. (d) Pérez-Juste, J.; Liz-Marzán, L. M.; Carnie, S.; Chan, D. Y. C.; Mulvaney, P. *Adv. Funct. Mater.* **2004**, *14*, 571. (e) Wang, Z.; Mohamed, M. B.; Link, S.; El-Sayed, M. A. *Surf. Sci.* **1999**, *440*, L809. (f) Gai, P. L.; Harmer, M. A. *Nano Lett.* **2002**, *2*, 771.
- (9) (a) Kim, F.; Song, J. H.; Yang, P. *J. Am. Chem. Soc.* **2002**, *124*, 14316. (b) Niidome, Y.; Nishiohara, K.; Hawasaki, H.; Yamada, S. *Chem. Commun.* **2003**, 2376. (c) Esumi, K.; Matsuhisa, K.; Torigoe, K. *Langmuir* **1995**, *11*, 1, 3285.
- (10) Sau, T. K.; Murphy, C. J. *Mater. Res. Soc. Symp. Proc.* **2004**, 789, 203.
- (11) (a) Kelly, K. L.; Coronado, E.; Zhao, L. L.; Schatz, G. C. *J. Phys. Chem. B* **2003**, *107*, 668. (b) Sosa, I. O.; Noguez, C.; Barrera, R. G. *J. Phys. Chem. B* **2003**, *107*, 6269.
- (12) Jin, R.; Cao, Y.; Hao, E.; Métraux, G. S.; Schatz, G. C.; Mirkin, C. A. *Nature* **2003**, *425*, 487.
- (13) Germain, V.; Brioude, A.; Ingert, D.; Pileni, M. P. *J. Chem. Phys.*, accepted for publication.
- (14) Salzemann, C.; Lisiecki, I.; Brioude, A.; Urban, J.; Pileni, M. P. *J. Phys. Chem. B*, in press.
- (15) Creighton, J. A.; Eaton, D. G. *J. Chem. Soc., Faraday Trans.* **1991**, *87*, 3881.
- (16) Wang, D.-S.; Kerker, M. *Phys. Rev.* **1981**, *B24*, 1777.
- (17) Purcell, E. M.; Pennypacker, C. R. *Astrophys. J.* **1973**, *186*, 705.
- (18) Lynch, D. W.; Hunter, W. R. In *Handbook of Optical Constants of Solids*; Palik, E. D., Ed.; Academic Press: New York, 1985; pp 350–356.
- (19) Draine, B. T.; Goodman, J. J. *Astrophys. J.* **1993**, *405*, 685.
- (20) Draine, B. T.; Flatau, P. J. *J. Opt. Soc. Am. A* **1994**, *11*, 1491.
- (21) Al-Sayed, A.-M.; Majied, A.-S. *Colloids Surf., A* **2004**, *246*, 61.
- (22) Mohamed, M. B.; Ismail, K. Z.; Link, S.; El-Sayed, M. A. *J. Phys. Chem. B* **1998**, *102*, 9370.
- (23) Yan, B.; Yang, Y.; Wang, Y. *J. Phys. Chem. B* **2003**, *107*, 9159.
- (24) Lebedeva, V. N.; Distler, G. I. *Opt. Spectrosc.* **1967**, *23*, 527.
- (25) Skillman, D. C.; Berry, C. R. *J. Chem. Phys.* **1968**, *48*, 3297.
- (26) Kelly, K. L.; Lazarides, A. A.; Shatz, G. C. *Comput. Sci. Eng.* **2001**, *3*, 67.
- (27) Transmission electron microscope (TEM) images are obtained using a JEOL 100 CXII instrument at 100 kV. Absorption spectra are recorded from aqueous solution by using a CARY 5G UV–vis–NIR spectrophotometer (Varian).